

# Extendable Long-Horizon Planning via Hierarchical Multiscale Diffusion

Chang Chen<sup>\*1</sup> Hany Hamed<sup>\*2</sup> Doojin Baek<sup>2</sup> Taegu Kang<sup>2</sup> Yoshua Bengio<sup>3</sup> Sungjin Ahn<sup>2,4</sup>

## Abstract

This paper tackles a novel problem, extendable long-horizon planning—enabling agents to plan trajectories longer than those in training data without compounding errors. To tackle this, we propose the Hierarchical Multiscale Diffuser (HM-Diffuser) and Progressive Trajectory Extension (PTE), an augmentation method that iteratively generates longer trajectories by stitching shorter ones. HM-Diffuser trains on these extended trajectories using a hierarchical structure, efficiently handling tasks across multiple temporal scales. Additionally, we introduce Adaptive Plan Pondering and the Recursive HM-Diffuser, which consolidate hierarchical layers into a single model to process temporal scales recursively. Experimental results demonstrate the effectiveness of our approach, advancing diffusion-based planners for scalable long-horizon planning.

## 1. Introduction

The ability to plan over long horizons (Hamrick et al., 2020; Mattar & Lengyel, 2022) enables agents to make decisions aligned with long-term goals, even under sparse rewards (Silver et al., 2016; Hafner et al., 2019; Hansen et al., 2022). However, building effective world models (Ha & Schmidhuber, 2018) for such planning is challenging due to the complexity of modeling high-dimensional dynamics. Traditional planning methods, which rely on autoregressive forward dynamics models, suffer from compounding errors (Lambert et al., 2022; Bachmann & Nagarajan, 2024), degrading performance over extended horizons.

The Diffuser approach (Janner et al., 2022; Ajay et al., 2022), leveraging Diffusion Models (Sohl-Dickstein et al., 2015; Ho et al., 2020), offers a promising alternative by eliminating forward dynamics models. Instead of sequential predictions, Diffuser generates entire trajectories holistically, akin

to image diffusion models, addressing error compounding and improving long-horizon planning accuracy.

While Diffuser is highly effective for long-horizon planning, it faces notable limitations. A primary issue is that its planning horizon is restricted by the trajectory lengths present in the training data, making it challenging to model trajectories longer than those encountered during training. However, in many applications, the ability to plan beyond the sequence length directly experienced is essential. In contrast, planning with forward models can extend the horizon to previously unseen lengths by rolling out longer sequences, although this introduces compounding of errors over time.

One solution is to collect longer trajectories, but this greatly reduces practicality. For instance, enabling a robot to plan at a week- or month-long horizon would require collecting trajectories of that length and training a Diffuser on them—an approach that is highly impractical with the current framework. Even if such trajectories were collected, planning performance is known to degrade on extended sequences (Chen et al., 2024c), and they would represent only a small fraction of the possible long-horizon planning space.

In this paper, we pose the following question: “How can we plan over horizons significantly longer than those available in the training data without suffering from compounding errors?” We refer to this challenge as *extendable long-horizon planning*. To tackle this, we propose a two-fold approach: (1) extending short training trajectories into longer ones through a method we term Progressive Trajectory Extension (PTE), and (2) incorporating a hierarchical multiscale structure into the Diffuser framework to efficiently train a diffusion planner on these extended trajectories.

Specifically, we introduce Progressive Trajectory Extension (PTE), a novel augmentation method that iteratively generates longer trajectories by stitching together previously extended trajectories over multiple rounds. However, we observe that the standard Diffuser struggles to perform well on such extended horizons, making a hierarchical approach, such as Hierarchical Diffuser (Chen et al., 2024c;a), a better fit. Building on this, we propose a new model, the Hierarchical Multiscale Diffuser (HM-Diffuser), which trains on extended trajectories by breaking down planning tasks across multiple temporal scales, enabling efficient training and execution for very long horizons.

<sup>\*</sup>Equal contribution <sup>1</sup>Rutgers University <sup>2</sup>KAIST <sup>3</sup>Mila <sup>4</sup>New York University. Correspondence to: Chang Chen <chang.chen@rutgers.edu>, Hany Hamed <h.hamed@kaist.ac.kr>.

To address the limitations of traditional Hierarchical Diffuser frameworks, which require separate Diffuser models for each hierarchy layer, we further introduce Adaptive Plan Pondering and the Recursive HM-Diffuser. These innovations distill the hierarchical layers into a single Diffuser model capable of recursively handling multiple temporal scales. Our results demonstrate the effectiveness of this approach in various long-horizon planning tasks, highlighting its potential to significantly advance efficient and scalable long-horizon decision-making.

This paper makes three contributions. First, we introduce extendable long-horizon planning in Diffuser, enabling trajectory generation beyond training lengths. Second, we propose the Hierarchical Multiscale Diffusion framework, combining Progressive Trajectory Extension (PTE) for iterative trajectory extension and the Recursive Hierarchical Diffuser for efficient long-horizon planning. Lastly, we introduce the Plan Extendable Trajectory Suite (PETS), a comprehensive suite of benchmarks including Extendable-Large, Giant, XXL Large Mazes, Extendable-Gym-MuJoCo, and Extendable-Kitchen, which addresses the lack of benchmarks for this task and advances diffusion-based planning.

## 2. Preliminaries

**Diffusion Models** (Sohl-Dickstein et al., 2015; Ho et al., 2020), inspired by the modeling of diffusion processes in statistical physics, are latent variable models with the following generative process  $p_\theta(\mathbf{x}_0) := \int p_\theta(\mathbf{x}_{0:M}) d\mathbf{x}_{1:M} =$

$$p_\theta(\mathbf{x}_0) = \int p(\mathbf{x}_M) \prod_{m=1}^M p_\theta(\mathbf{x}_{m-1} | \mathbf{x}_m) d\mathbf{x}_{1:M}. \quad (1)$$

Here,  $\mathbf{x}_0$  is a datapoint and  $\mathbf{x}_{1:M}$  are latent variables of the same dimensionality as  $\mathbf{x}_0$ . A diffusion model consists of two core processes: the reverse process and the forward process. The reverse process is defined as

$$p_\theta(\mathbf{x}_{m-1} | \mathbf{x}_m) := \mathcal{N}(\mathbf{x}_{m-1} | \boldsymbol{\mu}_\theta(\mathbf{x}_m, m), \sigma_m \mathbf{I}). \quad (2)$$

This process transforms a noise sample  $\mathbf{x}_M \sim p(\mathbf{x}_M) = \mathcal{N}(0, \mathbf{I})$  into an observation  $\mathbf{x}_0$  through a sequence of denoising transitions  $p_\theta(\mathbf{x}_{m-1} | \mathbf{x}_m)$  for  $m = M, \dots, 1$ . Conversely, the forward process defines the approximate posterior  $q(\mathbf{x}_{1:M} | \mathbf{x}_0) = \prod_{m=0}^{M-1} q(\mathbf{x}_{m+1} | \mathbf{x}_m)$  via the forward transitions:

$$q(\mathbf{x}_{m+1} | \mathbf{x}_m) := \mathcal{N}(\mathbf{x}_{m+1}; \sqrt{\alpha_m} \mathbf{x}_m, (1 - \alpha_m) \mathbf{I}). \quad (3)$$

The forward process iteratively applies this transition from  $m = 0, \dots, M - 1$  according to a predefined variance schedule  $\alpha_1, \dots, \alpha_M$  and gradually transforms the observation  $\mathbf{x}_0$  into noise  $\mathcal{N}(0, \mathbf{I})$  as  $m \rightarrow M$  for a sufficiently large  $M$ . Unlike the reverse process involving

learnable model parameters  $\theta$ , the forward process is predefined without learning parameters. Learning the parameter  $\theta$  of the reverse process is done by optimizing the variational lower bound on the log likelihood  $\log p_\theta(\mathbf{x}_0)$ . Ho et al. (2020) demonstrated that this can be achieved by minimizing the following simple denoising objective:  $\mathcal{L}(\theta) = \mathbb{E}_{\mathbf{x}_0, m, \epsilon} [\|\epsilon - \epsilon_\theta(\mathbf{x}_m, m)\|^2]$ . Specifically, this is to make  $\epsilon_\theta(\mathbf{x}_m, m)$  predict the noise  $\epsilon \sim \mathcal{N}(0, \mathbf{I})$  that was used to corrupt  $\mathbf{x}_0$  into  $\mathbf{x}_m = \sqrt{\bar{\alpha}_m} \mathbf{x}_0 + \sqrt{1 - \bar{\alpha}_m} \epsilon$ . Here,  $\bar{\alpha}_m = \prod_{i=0}^m \alpha_i$ .

**Planning with Diffusion.** A prominent approach to planning via diffusion has recently gained increasing attention, with Diffuser (Janner et al., 2022) being one of the most well-known methods. Diffuser formulates planning as a trajectory generation problem using diffusion models, first training a diffusion model  $p_\theta(\tau)$  on offline trajectory data  $\tau = (s_0, a_0, s_1, a_1, \dots, s_T, a_T)$  and then guiding sampling toward high-return trajectories using a classifier guided approach (Dhariwal & Nichol, 2021). This guidance model,  $p_\phi(\mathbf{y} | \tau) \propto \exp(G_\phi(\mathbf{x}))$ , predicts trajectory returns, modifying the sampling distribution to  $\tilde{p}_\theta(\tau) \propto p_\theta(\tau) \exp(\mathcal{J}_\phi(\tau))$ , which biases the denoising process toward optimal trajectories at test time. To ensure generated trajectories start at the current state, Diffuser enforces  $s_0 = s$  during denoising, while in goal-conditioned tasks,  $s_T = s_g$  is enforced to reach the target.

## 3. Proposed Method

Our primary goal is to develop a planner capable of handling planning horizons far longer than those available in the dataset. To achieve this, we introduce a two-phase approach: first, we extend shorter trajectories into longer ones using a novel method called Progressive Trajectory Extension (PTE). Second, we propose a hierarchical multiscale planner designed to learn effectively from these extended trajectories, significantly improving its long-horizon planning capabilities.

### 3.1. Progressive Trajectory Extension

Progressive Trajectory Extension (PTE) process iteratively extends trajectories through successive rounds. Before initiating a PTE round, several key modules must be trained. These include a diffusion model  $p_\theta^{\text{stitcher}}(\tau)$ , referred to as the *stitcher*. The stitcher is trained on the base trajectory dataset  $\mathcal{D}^0$  and generates plans of length  $h$ . Notably, the base dataset  $\mathcal{D}^0$  consists solely of short trajectories directly collected from the environment. The training process of the stitcher resembles that of an unconditional diffuser (Janner et al., 2022), but it is specifically adapted to operate on state sequences. Additionally, we train an inverse dynamics model  $a_t = f_\theta^a(s_t, s_{t+1})$  to infer actions, and a reward prediction model  $r_t = f_\theta^r(s_t, a_t)$  is trained to estimate rewards.

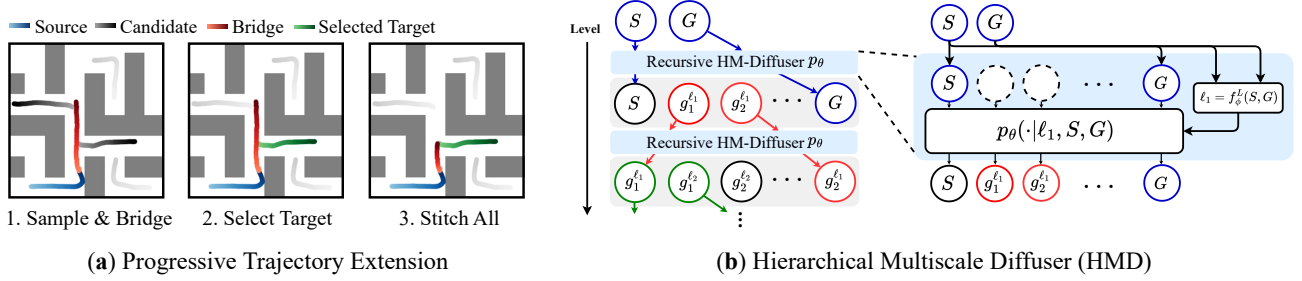


**Figure 1: (a) Progressive Trajectory Extension** involves the following steps. 1. Sample and Bridge: Sampling a source trajectory and multiple candidate trajectories. Using a pre-trained stitcher to extend the source trajectory while filtering out unreachable candidates. 2. Select Target: Choosing a target trajectory from the remaining candidates. 3. Stitch All: Using the stitcher again to bridge the gap between the source endpoint and the target start, completing one extension iteration. **(b) Hierarchical Multiscale Diffuser (HMD)** utilizes a shared model at each level. Assisted by the pretrained pondering depth predictor  $f_\phi^L$ , HMD determines the appropriate resolution of subgoals. These subgoals are recursively fed back into the model until the entire trajectory is planned.

In the  $r$ -th extension round, PTE receives the two input datasets:  $\mathcal{S}^r$  and  $\mathcal{T}^r$ . Because the trajectory extension is basically to connect two trajectories, we take a source trajectory from  $\mathcal{S}^r$  and a target trajectory from  $\mathcal{T}^r$ , respectively. Along with pretrained modules explained in the above, these datasets are used to generate an output dataset  $\mathcal{D}_{\text{out}}^r$ , which contains extended trajectories.

For the first round of extension,  $\mathcal{S}^1$  and  $\mathcal{T}^1$  are always set to the base dataset  $\mathcal{D}^0$ . For  $r > 1$ , we offer some flexibility in choosing  $\mathcal{S}^r$  and  $\mathcal{T}^r$ . For instance,  $\mathcal{S}^r$  may correspond to the output of the previous round, i.e.,  $\mathcal{S}^r = \mathcal{D}_{\text{out}}^{r-1}$ , while setting  $\mathcal{T}^r = \mathcal{D}^0$  as the default setting. For simplicity, we assume this default scenario in the following explanation. See Appendix section D for alternative configurations.

**Stitching Iterations.** As illustrated in Figure 1(a), PTE in each round consists of the following stitching iterations:

(i) *Sampling source, candidates, and bridge.* A source trajectory  $\tau^{\text{src}} \in \mathcal{S}^r$  is randomly sampled, along with a batch of candidate target trajectories  $\mathcal{T}_c \subset \mathcal{T}^r$ , where  $\tau_i^{\text{cand}} \in \mathcal{T}_c$ . To ensure high-quality extended trajectories, identifying optimal stitching points on source and target trajectories is crucial. However, an exhaustive grid search over all possible stitching points is computationally expensive. Instead, we approximate this process by probabilistically sampling stitching points and performing stitching on those segments. Specifically, the source trajectory is split into segments by sampling a last index  $t$ , and the truncated source trajectory up to  $t$  is used as  $\tau^{\text{src}}$ . Similarly, for each target  $\tau_i^{\text{cand}}$ , a starting index  $t'$  is sampled, and the segment from  $t'$  to the end is used as  $\tau_i^{\text{cand}}$ . The final state  $s_t^{\text{src}}$  of the source trajectory is used as the starting state for the bridge  $\tau^{\text{brg}}$ , sampled via the stitcher:  $\tau^{\text{brg}} \sim p_\theta^{\text{stitcher}}(\tau | s_0 = s_t^{\text{src}})$ .

(ii) *Selecting a target trajectory.* A set of *stitchable* candidates, denoted as  $\mathcal{T}_{\text{stitch}}$ , is constructed by evaluating the proximity between the source trajectory  $\tau^{\text{src}}$  and the candidate target segments  $\tau_i^{\text{cand}}$  for all  $i$ . Specifically, a candidate

trajectory  $\tau_i^{\text{cand}}$  is included in  $\mathcal{T}_{\text{stitch}}$  if the minimum distance (e.g., Euclidean or cosine similarity) between any state in the bridge trajectory  $\tau^{\text{brg}}$  and the starting state in  $\tau_i^{\text{cand}}$  is below a predefined threshold. Finally, a target trajectory  $\tau^{\text{tgt}}$  is sampled from the set of stitchable candidates  $\mathcal{T}_{\text{stitch}}$ .

(iii) *Stitching the source and target.* To ensure the quality of the bridge trajectory, it is resampled using conditional generation, following (Li et al., 2024). That is, we first calculate the number of steps needed to connect  $s_0^{\text{brg}} = s_t^{\text{src}}$  to the target trajectory  $\tau^{\text{tgt}}$ . Specifically, the stepwise distance  $k$  is defined as the number of steps between  $s_0^{\text{brg}}$  and  $s_{t'}^{\text{brg}}$ , where  $s_{t'}^{\text{brg}}$  represents the state in  $\tau^{\text{brg}}$  that is closest to the starting state  $s_0^{\text{tgt}}$  of the target trajectory  $\tau^{\text{tgt}}$ . Finally, the refined bridge trajectory is sampled from  $p_\theta^{\text{stitcher}}$ , conditioned on  $s_t^{\text{src}}$  and the  $h - k + 1$  goal states from the target:  $\tau^{\text{rebrg}} \sim p_\theta^{\text{stitcher}}(\tau | s_0 = s_t^{\text{src}}, s_{k:h} = s_{0:h-k}^{\text{tgt}})$ .

As a result of the above process, a new extended trajectory is generated:  $\tau^{\text{new}} = [\tau^{\text{src}}, \tau_{0:k-1}^{\text{rebrg}}, \tau^{\text{tgt}}]$ , where square brackets denote concatenation. The extended trajectory  $\tau^{\text{new}}$  is added to  $\mathcal{D}_{\text{out}}^r$ , completing one extension iteration. This process repeats until  $\mathcal{D}_{\text{out}}^r$  reaches the desired dataset size. To ensure trajectories grow progressively longer over successive rounds, we also introduce the following techniques:

**Tail-to-Head Stitching** is an intuitive method for extending trajectories by connecting the end of a source trajectory to the beginning of a target trajectory. This method assigns higher probabilities to the tail of the source trajectory when sampling the last index  $t$ , and to the head of the target trajectory when sampling the starting index  $t'$ . Setting uniform probabilities replicates standard stitching behavior, making this method both simple and adaptable for various use cases.

**Linear and Exponential PTE.** The PTE method allows for flexible design by controlling the source and target trajectory datasets. We introduce two variations: The first, Linear PTE, serves as the base method, extending trajectory lengths linearly over successive rounds. This is achieved by restrict-

ing the target dataset to always be the base dataset, defined as  $\mathcal{S}^r = \mathcal{D}_{\text{out}}^{r-1}$  and  $\mathcal{T}^r = \mathcal{D}^0$ . As a result, the trajectory length grows incrementally in each round, ensuring a steady and manageable extension process.

However, the linear growth rate may require multiple rounds of stitching to generate significantly longer trajectories, especially in large environments. To overcome this limitation, we propose Exponential PTE, which accelerates trajectory growth by using the union of all previous output datasets as both the source and target datasets. Formally, this is defined as  $\mathcal{S}^r = \mathcal{T}^r = \mathcal{D}_{\text{out}}^{r-1}$ . By leveraging these progressively expanded datasets, Exponential PTE facilitates rapid trajectory extension, making it more efficient for large-scale environments. However, this approach may result in a sparser length span compared to Linear PTE, as the focus shifts towards generating longer trajectories more quickly.

After  $R$  rounds of trajectory stitching, we obtain a series of datasets where the average trajectory length increases with each round. These datasets are then merged into a single dataset  $\mathcal{D}$ , containing trajectories of varying lengths.

### 3.2. Hierarchical Multiscale Diffusers

A straightforward approach to obtaining a planner from the extended dataset  $\mathcal{D}$  is to train a standard Diffuser (Janner et al., 2022; Ajay et al., 2022). However, handling the very long trajectories of PTE significantly increases the model’s output dimensionality, leading to substantial computational overhead. Prior studies (Chen et al., 2024c) indicate that Diffuser performance declines as planning horizons grow.

To address this issue, we propose leveraging Hierarchical Diffuser (HD) (Chen et al., 2024c), taking advantage of its structured planning mechanism to improve efficiency and scalability. Specifically, our planner consists of a hierarchy of  $L$ -level planners, denoted as  $p_{\theta_\ell}(\tau)$  for  $\ell = 1, \dots, L$ . Each planner at level  $\ell$  is characterized by a jump length  $j_\ell$  and a jump count  $k_\ell$ . The trajectory length at level  $\ell$  is defined as  $H_\ell = j_\ell \times k_\ell$ , with trajectories randomly sampled from  $\mathcal{D}$ . Instead of utilizing all trajectory states, the planner sparsely selects every  $j_\ell$ -th state over  $k_\ell$  steps, maintaining an effective receptive horizon of  $H_\ell$  while significantly reducing output dimensionality for computational efficiency. These selected states, referred to as *subgoals*, are denoted as  $g_1^\ell, \dots, g_{k_\ell}^\ell$ . The lowest level,  $\ell = 1$ , is set with a jump length of  $j_1 = 1$ , producing a short, dense plan.

The core idea of hierarchical planning in HD is that at level  $\ell$ , the trajectory is conditioned on two consecutive subgoals from the higher level  $\ell + 1$ : the first subgoal acts as the starting point, while the second defines the end-point. Specifically, given two consecutive subgoals  $g_t^{\ell+1}$  and  $g_{t+1}^{\ell+1}$ , the planned trajectory at level  $\ell$  is defined as

$g_t^{\ell+1}, g_1^\ell, g_2^\ell, \dots, g_{k_\ell}^\ell, g_{t+1}^{\ell+1}$ , which is sampled from:

$$p_{\theta_\ell}(\tau | g_0^\ell = g_t^{\ell+1}, g_{k_\ell-1}^\ell = g_{t+1}^{\ell+1}) \quad (4)$$

This hierarchical structure ensures that lower-level planners refine the trajectory while adhering to the broader constraints set by the higher-level subgoals. To maintain this consistency, we enforce  $H_\ell = j_{\ell+1}$ , ensuring that each jump segment at the higher level is decomposed into  $k_\ell$  subgoals at the lower level.

#### 3.2.1. ADAPTIVE PLAN PONDERING

One key issue of the above approach is that planning always starts from the highest level  $L$  and progresses downward to generate the final action. This becomes inefficient when the goal is much closer than the highest planning length  $H_L$ , often resulting in unnecessary detours. To address this, we introduce Adaptive Plan Pondering (APP), which dynamically adjusts the starting level based on the proximity of the goal. We train a pondering depth predictor  $\hat{\ell} = f_\phi^L(s_0, s_g)$  that, given the start and goal states, predicts the optimal planning level. Since the hierarchy level of each trajectory in  $\mathcal{D}$  is known during training, this predictor can be trained straightforwardly. At test time, APP allows planning to start from a lower level when appropriate, bypassing unnecessary higher-level steps. This optimizes efficiency by preventing detours and reducing computational overhead.

#### 3.2.2. RECURSIVE HM-DIFFUSER

Another key inefficiency is the need to maintain multiple separate diffuser models,  $p_{\theta_1}, \dots, p_{\theta_L}$ , each with its own set of parameters. This raises an important question: can a single diffusion model effectively handle all levels of the hierarchy? While sharing parameters may not necessarily improve performance compared to non-shared models with larger capacity, it significantly simplifies model management and reduces computational complexity, making it a desirable approach if performance can be maintained.

To address this, we introduce Recursive Hierarchical Multiscale Planning to HMD, enabling a single diffusion model to handle the entire hierarchy, as illustrated in Figure 1(b). Instead of maintaining separate diffusers for each level, we replace them with a single level-conditioned diffusion model  $p_\theta(\tau | \ell)$ . To accommodate different planning levels, the model’s output dimensionality is set to  $\bar{d} = \max d_\ell$ , where  $d_\ell = (k_\ell + 1) \times \dim(s_t)$  represents the output dimension of the  $\ell$ -th diffuser.

During training, the shared diffuser  $p_\theta(\tau | \ell)$  is optimized by randomly sampling  $\ell \sim \text{uniform}(1, \dots, L)$  to generalize across all levels. For planning, the process starts at the appropriate level determined by APP. Once an initial sequence of subgoals is generated, each pair of consecutive subgoals is recursively fed back into the same diffuser at the next



lower level. Specifically, the first and last subgoals of the previous plan serve as the start and end states, respectively, while the level indicator is reduced by one:

$$p_{\theta}(\tau|\ell, g_0^{\ell} = g_t^{\ell+1}, g_{k_{\ell}-1}^{\ell} = g_{t+1}^{\ell+1}). \quad (5)$$

This process continues iteratively until reaching the lowest level. Refer to Appendix B for details.

## 4. Related Work

**Diffusion-based Planners in Offline RL.** Diffusion models are powerful generative models that frame data generation as an iterative denoising process (Ho et al., 2020; Song et al., 2020). They were first introduced in reinforcement learning as planners by (Janner et al., 2022), utilizing their sequence modeling capabilities. Subsequent work (Ajay et al., 2022; Liang et al., 2023; Rigter et al., 2023) has shown promising results in offline-RL tasks. Diffusion models have also been explored as policy networks to model highly multi-modal behavior policies (Wang et al., 2023; Kang et al., 2024). Recent advancements have extended these models to hierarchical architectures (Wenhao Li & Zha, 2023; Chen et al., 2024c; Dong et al., 2024; Chen et al., 2024a), proving effective for long-horizon planning. Our method builds on this by not only using diffusion models for extremely long planning horizons but also exploring the stitching of very short trajectories with diffusion models.

**Data Augmentation in RL** has been a crucial strategy for improving generalization in offline RL. Previous work has used dynamic models to stitch nearby states from trajectories (Char et al., 2022), generate new transitions (Hepburn & Montana, 2022), or create entire trajectories from sampled initial states (Zhou et al., 2023; Lyu et al., 2022; Wang et al., 2021; Zhang et al., 2023). More recently, diffusion models have been applied for augmentation (Zhu et al., 2023b). (Lu et al., 2023) used diffusion models to capture the joint distribution of transition tuples, while (He et al., 2024) extended this to multi-task settings. (Li et al., 2024) used diffusion to connect trajectories through inpainting. Additional related works on hierarchical planning is provided in Appendix A.

## 5. Experiments

In this section, we aim to answer these questions: (1) Can PTE generate plausible trajectories significantly longer than those in the training dataset? (2) Is HMD capable of creating feasible plans for tasks requiring much longer planning horizons than those seen in training? (3) Does it remain effective in high-dimensional manipulation tasks? (4) Lastly, is our framework still effective when a long planning horizon is unnecessary? To facilitate our analysis, we introduce the Plan Extendable Trajectory Suite (PETS), which includes extendable dataset from Maze2D, Gym-MuJoCo, and FrankaKitchen environment.

Throughout the experiment section, we denote baselines trained on the extended dataset  $\mathcal{D}$  generated by PTE with the -X suffix, highlighting their ability to perform long-horizon planning through the incorporation of the extended dataset. In contrast, baselines trained only on the short base dataset do not include this suffix. For implementation details, please refer to Appendix B. Our code will be made publicly available upon acceptance.

### 5.1. Analysis on the Progressive Trajectory Extension

To address our first question, we conduct illustrative experiments in the Maze2D environment. We tested the effectiveness of our proposed Progressive Trajectory Extension (PTE) process for long-horizon extension in larger mazes. Specifically, we used the Large Maze from D4RL, the Giant Maze from (Park et al., 2024), and designed a new XXLarge Maze with a larger layout as shown in Figure C.5, which we refer to as the Extendable Maze2D benchmark.

**Datasets.** Existing benchmarks are unrealistic because, in practice, collecting long-horizon data is inherently challenging. To address this, our Extendable Maze2D benchmark is designed around short base trajectories, reflecting the reality that short-horizon data is much easier to collect. For data collection, we randomly sample start and goal locations within five maze cells to ensure short trajectories. Following D4RL, we collected one million transitions for each Maze setting, as depicted in Figure C.5.

**Linear PTE and Exponential PTE.** As discussed earlier, being a flexible trajectory extension mechanism, depending on the input dataset, we can extend the trajectory either linearly or exponentially. We applied both extension strategies on the collected short base trajectories. As shown in Figure 2(a), Linear PTE method gradually increases trajectory length, making it suitable for more stable trajectory extension. However, it may be less efficient in scenarios requiring long-horizon planning, such as in the Large, Giant, and XXLarge mazes. In contrast, Exponential PTE rapidly extends trajectory lengths, providing an effective solution for managing longer trajectories. Figure 2(b) demonstrates the effectiveness of our PTE methods, covering significant portion of possible start-goal pairs in the XXLarge maze. Figure 2(c) presents a progressive view of both PTE methods over multiple rounds. Notably, starting from the top-left corner of the maze, the extended trajectories using Exponential PTE nearly span the entire XXLarge maze by the third round, highlighting its efficiency in rapid trajectory expansion.

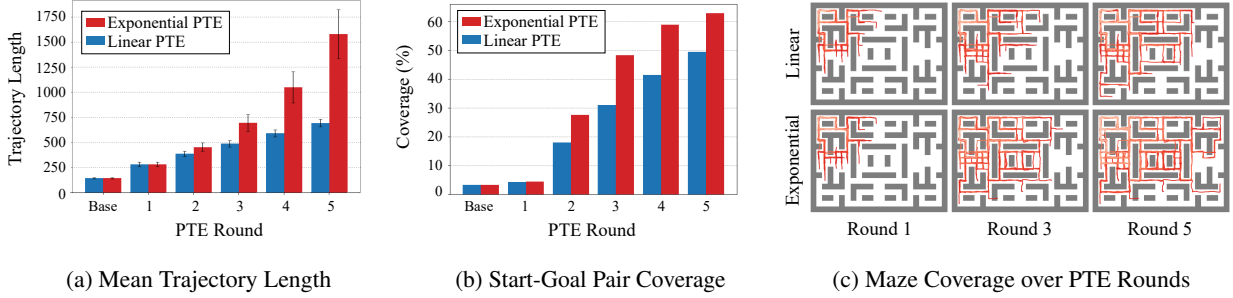


**Figure 2: Progressive Trajectory Extension Results.** (a) Mean trajectory lengths for the XXLLarge maze. Linear PTE increases trajectory length at a constant rate, while Exponential PTE grows exponentially across rounds. (b) Start-goal pair coverage improves as PTE progresses, with Exponential PTE covering a significantly larger portion of the maze compared to Linear PTE. (c) Visualization of maze coverage of the XXLLarge maze over PTE rounds. Exponential PTE enables faster coverage expansion than Linear PTE.

## 5.2. Long-Horizon Planning

### 5.2.1. HM-DIFFUSER ON EXTENDABLE MAZE2D

**Datasets.** We start with the short base dataset and apply  $R = 7$  rounds of linear PTE to iteratively generate extended datasets. These datasets are then aggregated into a single dataset,  $\mathcal{D}$ , which contains trajectories of varying lengths, enhancing both diversity and generalization. Following Diffuser, we evaluate performance under two settings. In the single-task setting (Maze2D), the goal position remains fixed at the bottom-right corner of the maze while the starting position is randomized, testing the model’s ability to generate trajectories from diverse initial conditions. In contrast, the multi-task setting (Multi2D) randomizes both the start and goal positions. This increased variation in planning scenarios enables a more rigorous evaluation of the model’s capacity to generalize across a broader range of tasks.

**Baselines.** We train Diffuser, HD, and our proposed Hierarchical Multiscale Diffuser (HM-Diffuser) using the extended dataset  $\mathcal{D}$ , denoting these models with the -X suffix. To assess the impact of PTE on long-horizon planning, we also compare them against a Diffuser trained only on the short base dataset.

**Evaluation.** We report the mean and standard error over  $N = 200$  planning seeds. Performance is measured using the normalized scores, scaled by a factor of 100 (Fu et al., 2020; Janner et al., 2022). Following the Diffuser evaluation protocol, a PD controller is used during evaluation to execute planned trajectories. However, we observed that the PD controller makes the goal reachable even when the planned trajectories are very poor (Refer to Figure C.6 in Appendix for an illustrative example). To ensure that performance primarily reflects the model’s planning capabilities rather than controller interventions, we restrict the PD controller to be callable only when the agent are near the goal.

Table 1 demonstrates that HMD-X consistently outperforms all baselines across both settings. In the single-task set-

**Table 1: Maze2D Performance.** We compare the performance of baselines in single-task (Maze2D) and multi-task (Multi2D) settings in various maze environments (Large, Giant, and XXLLarge). The -X baselines are trained with the extended dataset consists of the union of 7 rounds of Linear PTE, while Diffuser is only trained with the short base dataset. We report the mean and the standard error over 200 planning seeds. HMD-X consistently outperforms all baselines across all settings.

Environment		Diffuser	Diffuser-X	HD-X	HMD-X
Maze2D	Large	$45.8 \pm 5.9$	$114.4 \pm 4.7$	$144.3 \pm 3.3$	<b><math>166.9 \pm 4.6</math></b>
Maze2D	Giant	$77.2 \pm 11.7$	$114.6 \pm 9.10$	$138.4 \pm 9.6$	<b><math>177.4 \pm 11.9</math></b>
Maze2D	XXLLarge	$14.1 \pm 4.9$	$23.0 \pm 3.4$	$56.4 \pm 4.9$	<b><math>82.1 \pm 8.5</math></b>
Single-task Average		45.7	84.0	113.0	<b>142.1</b>
Multi2D	Large	$33.4 \pm 5.9$	$130.3 \pm 4.0$	$150.3 \pm 3.0$	<b><math>174.7 \pm 3.8</math></b>
Multi2D	Giant	$77.8 \pm 11.8$	$140.2 \pm 8.9$	$168.8 \pm 9.0$	<b><math>246.7 \pm 10.6</math></b>
Multi2D	XXLLarge	$23.4 \pm 6.3$	$63.2 \pm 5.2$	$71.9 \pm 5.5$	<b><math>109.9 \pm 8.4</math></b>
Multi-task Average		44.9	111.2	130.4	<b>177.1</b>

ting, HMD-X achieves the highest average score (142.1), highlighting the effectiveness of its hierarchical and multiscale planning capabilities. Meanwhile, Diffuser-X, despite being trained on the extended dataset, struggles in the XXLLarge maze environment, achieving only  $23.0 \pm 3.4$ —a performance comparable to Diffuser trained solely on the base dataset. This suggests that Diffuser-X faces challenges in modeling long-horizon plans in complex environments. However, HD-X and HMD-X manage to retain better performance, demonstrating the effectiveness of the hierarchical planning. In the multi-task setting, HMD-X outperform all baselines, achieving an average score of 177.1, further demonstrating its ability to generalize across diverse tasks.

We observe that all the baselines trained with the extended dataset (denoted with the -X suffix) achieve higher performance than Diffuser, which was trained only with the base dataset. These results confirm that our proposed PTE framework and HM-Diffuser can effectively plan over substantially longer horizons than those exists in the short base dataset. For results using other rounds, refer to Figure C.7 in Appendix.

**Table 2: Comparison of HMD performance in the Maze2D-XXLarge environment, evaluating different PTE strategies.** The table presents results for varying rounds of PTE (5 and 7) and differing amounts of data collected per round.

R	Linear			Exponential		
	1M	2M	4M	1M	2M	4M
5	68.9 $\pm$ 7.2	69.6 $\pm$ 7.4	70.1 $\pm$ 7.7	53.4 $\pm$ 6.7	94.7 $\pm$ 8.0	115.4 $\pm$ 7.9
7	82.1 $\pm$ 8.5	86.4 $\pm$ 8.3	89.9 $\pm$ 8.2	30.0 $\pm$ 5.5	51.3 $\pm$ 6.7	120.5 $\pm$ 8.6

### 5.2.2. ABLATION STUDIES

In Figure 3 (a), we qualitatively illustrate the multiscale planning capability of HM-Diffuser, conditioned on different levels, where  $l = 1$  represents the lowest level. With the appropriate level determined by the pondering depth predictor, HMD maintains effective planning without deterioration, as indicated by the green box in Figure 3 (a) (see Figure C.9 for additional examples). Additionally, Figure 3 (b) shows that Diffuser and HD generate inefficient plans with excessive detours due to their fixed planning horizon (refer to Figure C.10 for more examples). In Figure C.8, we illustrate the high-level plans generated by HMD when conditioned on the predicted level. Following this, HMD is recursively called at lower levels to generate the full plan.

Table 2 shows the impact of the amount of data collected per round and PTE strategy on HMD performance in Maze2D-XXLarge. Linear PTE shows steady improvements, reaching 89.9  $\pm$  8.2 (Round 7, 4M). In contrast, Exponential PTE exhibits greater sensitivity to dataset size: smaller datasets lead to performance drops, whereas larger datasets (4M) achieve the highest score (120.5  $\pm$  8.6). These results highlight that while Linear PTE ensures stable and consistent performance gains, Exponential PTE requires sufficient data scaling to achieve optimal performance.

### 5.3. FrankaKitchen

High-dimensional manipulation tasks present a distinct challenge for offline reinforcement learning, which is orthogonal to the long-horizon planning. To investigate how our proposed framework performs in this domain, we conducted experiments on the Kitchen task. Similarly to the Maze2D task, the original D4RL (Fu et al., 2020) FrankaKitchen offline data set was used to build our extendable kitchen benchmark. Starting with short, fixed-length segments, we applied one round of linear PTE process to create our extended Kitchen dataset. For details, see Appendix E.

Our results are presented in Table 3, where methods trained on our extended dataset are denoted by appending an -X to their names. As shown in the table, when trained on our extended data set, the performance of Diffuser X improved from an average score of 43.8 to 45.8. This can be attributed to the extended planning horizon, which helps the model to be less short-sighted. Moreover, both HMD-X

**Table 3: Results on Extended Kitchen and Gym-MuJoCo Dataset.** When trained on our extended dataset, the performance of Diffuser-X get improved in general. The introduce of recursive hierarchical structure improvements the performance further over Diffuser-X. Results are averaged over 15 planning seeds.

Environment		Diffuser	Diffuser-X	HD-X	HMD-X
Kitchen	Partial-v0	41.7 $\pm$ 3.2	43.3 $\pm$ 5.5	56.7 $\pm$ 5.8	56.7 $\pm$ 5.3
	Mixed-v0	45.8 $\pm$ 3.1	48.3 $\pm$ 4.7	53.3 $\pm$ 3.1	61.7 $\pm$ 3.1
Kitchen Average		43.8	45.8	55.0	59.2
Walker2d	MedReplay	22.8 $\pm$ 2.7	20.1 $\pm$ 4.3	30.2 $\pm$ 5.9	29.6 $\pm$ 4.8
Walker2d	Medium	58.1 $\pm$ 5.6	62.6 $\pm$ 6.4	66.5 $\pm$ 4.3	72.7 $\pm$ 2.5
Walker2d	MedExpert	82.3 $\pm$ 4.6	80.3 $\pm$ 3.7	80.8 $\pm$ 2.9	79.3 $\pm$ 2.3
Walker2d Average		54.4	54.3	59.2	60.5
Hopper	MedReplay	18.7 $\pm$ 3.0	34.5 $\pm$ 6.2	22.5 $\pm$ 3.1	37.3 $\pm$ 4.8
Hopper	Medium	45.6 $\pm$ 1.9	44.3 $\pm$ 3.5	44.1 $\pm$ 2.8	44.9 $\pm$ 3.5
Hopper	MedExpert	61.4 $\pm$ 8.4	74.9 $\pm$ 8.0	67.9 $\pm$ 7.7	74.3 $\pm$ 9.0
Walker2d Average		41.9	51.2	44.8	52.2

and HD-X significantly outperformed Diffuser-X due to their structured hierarchical planning, which reduces the dimensionality of the sequences, as also observed in Chen et al. (2024b). Among them, HMD-X slightly outperformed HD-X, with an average score of 59.2 versus 55.0. We hypothesize that this improvement might be due to the shared weights enhancing the underlying representation learning and forward dynamics model in the Kitchen task.

### 5.4. Gym-MuJoCo

Having demonstrated efficiency and effectiveness in the Extendable-Maze2D and Kitchen tasks, it is worth investigating whether our proposed framework could also benefit tasks where long-horizon planning is not necessary. To this end, we evaluate the performance of proposed framework on the Extendable-Gym-MuJoCo tasks with dense rewards. Similar to the Maze2D and Kitchen benchmarks, this new benchmark is also built from short segments derived from the standard D4RL dataset, extended with our linear PTE process. For details of the dataset generation, please refer to Appendix E. To highlight the effectiveness of PTE, we have filtered out tasks that do not require an extended planning horizon. Please refer to Table F.8 for details.

As shown in Table 3, when trained on the extended dataset, Diffuser-X’s average performance improved from 41.9 to 51.2 on the Hopper tasks, likely due to less short-sighted planning. On Walker2d, though no improvement is observed, we argue that the increased planning horizon and sequence dimensionality, which burden the Diffuser, would normally result in a performance drop (Chen et al., 2024b). However, on our extended dataset, Diffuser-X achieved comparable performance. HMD-X outperforms both Diffuser-X and its hierarchical counterpart, HD-X, on the Walker2d and Hopper tasks, with average scores of 60.5 and 52.2, respectively.

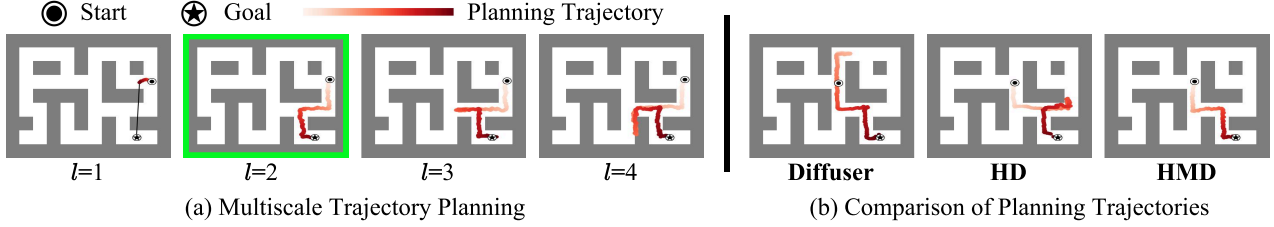


**Figure 3: Trajectory Planning Visualization.** (a) Multiscale trajectory planning using HMD with different levels ( $l$ ), where the figure highlighted with a green border indicates the level predicted by the pondering depth predictor. (b) Comparison of planning trajectories using different models (Diffuser, HD, and HMD), illustrating variations in trajectory planning efficiency and goal-reaching performance.

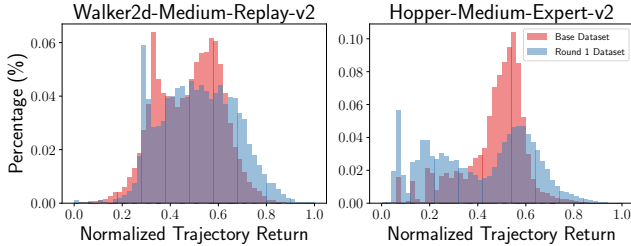


**Figure 4: Trajectory Return Distribution.** After one round of PTE, the distribution of trajectory returns expands to cover more areas within the range of high trajectory returns.

#### 5.4.1. ANALYSIS

Since long-horizon planning is not necessarily required in the Gym-MuJoCo and Kitchen tasks, it may not seem intuitive how our PTE would be beneficial. To investigate this, we compare the trajectory returns of the base dataset (short segments) to those of the extended dataset after one round of the PTE process. Because trajectory return generally increases with length, we plot the distribution of normalized trajectory returns in Figure 4. As depicted, it indicates an increase in the number of high-return trajectories. Since guidance sampling is employed to generate plans with potentially the highest expected returns, we hypothesize that this distributional shift helps in generating better plans.

#### 5.5. HMD on Standard Benchmark

Finally, we evaluate whether the proposed HMD outperforms baseline methods also on the standard D4RL benchmark. This is different from the previous experiments without PTE as the standard D4RL dataset contains the original longer trajectories. As shown in Table F.9, we can see that HMD outperforms all baselines.

### 6. Limitations & Discussion

While our method significantly improves long-horizon planning, several areas remain for further refinement. Progressive Trajectory Extension (PTE) occasionally produces overlapping or detoured trajectories and, in some cases, gener-

ates infeasible stitching, such as paths that appear to pass through obstacles. Although our experiments show that these imperfections do not hinder overall task performance, refining PTE for more reliable trajectory generation remains an important direction.

Additionally, we have not yet explored visual domain planning, such as image-based decision-making. However, most existing works in diffusion-based planning (Janner et al., 2022; Ajay et al., 2022) and hierarchical trajectory generation (Chen et al., 2024c;a) similarly operate in state-space representations rather than raw visual inputs, making this a common limitation in the field rather than a shortcoming of our specific approach. Nonetheless, extending HMD to handle high-dimensional visual observations would be an important step for real-world applications.

Another limitation is the lack of temporal state abstraction, which may be necessary for handling extremely long-horizon plans more efficiently by focusing on key decision points rather than every intermediate step.

Furthermore, our method lacks test-time compute mechanisms, restricting its ability to refine plans dynamically during execution. While replanning is possible, integrating search-based methods like Monte Carlo Tree Search (MCTS) could enable more adaptive and precise planning when additional computation time is available. Addressing these limitations will be essential for further advancing extendable long-horizon planning and expanding its real-world applicability.

### 7. Conclusion

In this work, we introduce the Hierarchical Multiscale Diffuser (HMD) framework for extendable long-horizon planning via diffusion models. Given a set of short trajectories that are insufficient for solving the target task, our method first extends these trajectories using Progressive Trajectory Extension (PTE). We then train an HMD planner on this augmented dataset, leveraging a hierarchical multiscale structure to efficiently generate long-horizon



plans. Our experiments demonstrate promising results on the long-horizon Maze2D task, as well as in complex, high-dimensional environments such as dense-reward Gym-MuJoCo and manipulation-based Kitchen tasks.

## Acknowledgement

This research was supported by GRDC (Global Research Development Center) Cooperative Hub Program (RS-2024-00436165) and Brain Pool Plus Program (No. 2021H1D3A2A03103645) through the National Research Foundation of Korea (NRF) funded by the Ministry of Science and ICT, and partly by the research support program of Samsung Advanced Institute of Technology.

## Impact Statement

This work introduces Hierarchical Multiscale Diffuser (HMD), a framework that extends diffusion-based planning to significantly longer horizons through hierarchical multi-scale modeling and Progressive Trajectory Extension (PTE). As a general-purpose planning framework, HMD does not inherently pose direct risks. However, careful consideration is required when applying it to safety-critical domains, where long-horizon decision-making impacts areas such as autonomous systems, robotics, and strategic planning. Depending on its implementation, HMD could influence high-stakes applications in fields like healthcare, finance, and logistics, necessitating safeguards to ensure reliability and alignment with ethical standards. Additionally, the increased computational demands of diffusion-based planning raise concerns about energy efficiency and sustainability, emphasizing the need for responsible and efficient AI deployment.

## References

- Ajay, A., Du, Y., Gupta, A., Tenenbaum, J., Jaakkola, T., and Agrawal, P. Is conditional generative modeling all you need for decision-making? *arXiv preprint arXiv:2211.15657*, 2022.
- Bachmann, G. and Nagarajan, V. The pitfalls of next-token prediction. *arXiv preprint arXiv:2403.06963*, 2024.
- Char, I., Mehta, V., Villafior, A., Dolan, J. M., and Schneider, J. Bats: Best action trajectory stitching. *arXiv e-prints*, pp. arXiv–2204, 2022.
- Chen, C., Baek, J., Deng, F., Kawaguchi, K., Gulcehre, C., and Ahn, S. PlanDQ: Hierarchical plan orchestration via d-conductor and q-performer. In *Forty-first International Conference on Machine Learning*, 2024a. URL <https://openreview.net/forum?id=17ZwoHl65h>.
- Chen, C., Deng, F., Kawaguchi, K., Gulcehre, C., and Ahn, S. Simple hierarchical planning with diffusion. In *The Twelfth International Conference on Learning Representations*, 2024b. URL <https://openreview.net/forum?id=kXHEBK9uAY>.
- Chen, C., Deng, F., Kawaguchi, K., Gulcehre, C., and Ahn, S. Simple hierarchical planning with diffusion. *arXiv preprint arXiv:2401.02644*, 2024c.
- Dhariwal, P. and Nichol, A. Diffusion models beat gans on image synthesis. *Advances in neural information processing systems*, 34:8780–8794, 2021.
- Dong, Z., Hao, J., Yuan, Y., Ni, F., Wang, Y., Li, P., and Zheng, Y. Diffuserlite: Towards real-time diffusion planning. *arXiv preprint arXiv:2401.15443*, 2024.
- Fu, J., Kumar, A., Nachum, O., Tucker, G., and Levine, S. D4RL: Datasets for deep data-driven reinforcement learning. *arXiv preprint arXiv:2004.07219*, 2020.
- Ha, D. and Schmidhuber, J. World models. *arXiv preprint arXiv:1803.10122*, 2018.
- Hafner, D., Lillicrap, T., Fischer, I., Villegas, R., Ha, D., Lee, H., and Davidson, J. Learning latent dynamics for planning from pixels. In *International conference on machine learning*, pp. 2555–2565. PMLR, 2019.
- Hafner, D., Lee, K.-H., Fischer, I., and Abbeel, P. Deep hierarchical planning from pixels. *arXiv preprint arXiv:2206.04114*, 2022.
- Hamrick, J. B., Friesen, A. L., Behbahani, F., Guez, A., Viola, F., Witherspoon, S., Anthony, T., Buesing, L., Veličković, P., and Weber, T. On the role of planning in model-based deep reinforcement learning. *arXiv preprint arXiv:2011.04021*, 2020.

- Hansen, N., Wang, X., and Su, H. Temporal difference learning for model predictive control. *arXiv preprint arXiv:2203.04955*, 2022.
- He, H., Bai, C., Xu, K., Yang, Z., Zhang, W., Wang, D., Zhao, B., and Li, X. Diffusion model is an effective planner and data synthesizer for multi-task reinforcement learning. *Advances in neural information processing systems*, 36, 2024.
- Hepburn, C. A. and Montana, G. Model-based trajectory stitching for improved offline reinforcement learning. In *3rd Offline RL Workshop: Offline RL as a "Launchpad"*, 2022. URL <https://openreview.net/forum?id=XsQLS6Ls5->.
- Ho, J., Jain, A., and Abbeel, P. Denoising diffusion probabilistic models. *Advances in Neural Information Processing Systems*, 33:6840–6851, 2020.
- Hu, E. S., Chang, R., Rybkin, O., and Jayaraman, D. Planning goals for exploration. In *The Eleventh International Conference on Learning Representations*, 2023. URL <https://openreview.net/forum?id=6qeBuZSo7Pr>.
- Janner, M., Du, Y., Tenenbaum, J., and Levine, S. Planning with diffusion for flexible behavior synthesis. In *International Conference on Machine Learning*, 2022.
- Kaiser, L., Babaeizadeh, M., Milos, P., Osinski, B., Campbell, R. H., Czechowski, K., Erhan, D., Finn, C., Koza-kowski, P., Levine, S., et al. Model-based reinforcement learning for atari. *arXiv preprint arXiv:1903.00374*, 2019.
- Kang, B., Ma, X., Du, C., Pang, T., and Yan, S. Efficient diffusion policies for offline reinforcement learning. *Advances in Neural Information Processing Systems*, 36, 2024.
- Lambert, N., Pister, K., and Calandra, R. Investigating compounding prediction errors in learned dynamics models. *arXiv preprint arXiv:2203.09637*, 2022.
- Li, G., Shan, Y., Zhu, Z., Long, T., and Zhang, W. Diff-stitch: Boosting offline reinforcement learning with diffusion-based trajectory stitching. *arXiv preprint arXiv:2402.02439*, 2024.
- Li, J., Tang, C., Tomizuka, M., and Zhan, W. Hierarchical planning through goal-conditioned offline reinforcement learning. *IEEE Robotics and Automation Letters*, 7(4): 10216–10223, 2022.
- Li, W., Wang, X., Jin, B., and Zha, H. Hierarchical diffusion for offline decision making. In *International Conference on Machine Learning*, 2023.
- Liang, Z., Mu, Y., Ding, M., Ni, F., Tomizuka, M., and Luo, P. AdaptDiffuser: Diffusion models as adaptive self-evolving planners. *arXiv preprint arXiv:2302.01877*, 2023.
- Lu, C., Ball, P. J., Teh, Y. W., and Parker-Holder, J. Synthetic experience replay. In *Thirty-seventh Conference on Neural Information Processing Systems*, 2023. URL <https://openreview.net/forum?id=6jNq1AY1Uf>.
- Lyu, J., Li, X., and Lu, Z. Double check your state before trusting it: Confidence-aware bidirectional offline model-based imagination. In Oh, A. H., Agarwal, A., Belgrave, D., and Cho, K. (eds.), *Advances in Neural Information Processing Systems*, 2022. URL <https://openreview.net/forum?id=3e3IQMLDSLp>.
- Mattar, M. G. and Lengyel, M. Planning in the brain. *Neuron*, 110(6):914–934, 2022.
- Park, S., Frans, K., Eysenbach, B., and Levine, S. Ogbench: Benchmarking offline goal-conditioned rl. *arXiv preprint arXiv:2410.20092*, 2024.
- Rigter, M., Yamada, J., and Posner, I. World models via policy-guided trajectory diffusion. *arXiv preprint arXiv:2312.08533*, 2023.
- Silver, D., Huang, A., Maddison, C. J., Guez, A., Sifre, L., Van Den Driessche, G., Schrittwieser, J., Antonoglou, I., Panneershelvam, V., Lanctot, M., et al. Mastering the game of go with deep neural networks and tree search. *nature*, 529(7587):484–489, 2016.
- Sohl-Dickstein, J., Weiss, E., Maheswaranathan, N., and Ganguli, S. Deep unsupervised learning using nonequilibrium thermodynamics. In *International Conference on Machine Learning*, pp. 2256–2265. PMLR, 2015.
- Song, J., Meng, C., and Ermon, S. Denoising diffusion implicit models. *arXiv preprint arXiv:2010.02502*, 2020.
- Wang, J., Li, W., Jiang, H., Zhu, G., Li, S., and Zhang, C. Offline reinforcement learning with reverse model-based imagination. *Advances in Neural Information Processing Systems*, 34:29420–29432, 2021.
- Wang, Z., Hunt, J. J., and Zhou, M. Diffusion policies as an expressive policy class for offline reinforcement learning. In *The Eleventh International Conference on Learning Representations*, 2023. URL <https://openreview.net/forum?id=AHvFDPi-FA>.
- Wenhao Li, Xiangfeng Wang, B. J. and Zha, H. Hierarchical diffusion for offline decision making. *Proceedings of the 40th International Conference on machine learning*, 2023.

- Zhang, J., Lyu, J., Ma, X., Yan, J., Yang, J., Wan, L., and Li, X. Uncertainty-driven trajectory truncation for data augmentation in offline reinforcement learning. In *ECAI 2023*, pp. 3018–3025. IOS Press, 2023.
- Zhou, Z., Zhu, C., Zhou, R., Cui, Q., Gupta, A., and Du, S. S. Free from bellman completeness: Trajectory stitching via model-based return-conditioned supervised learning. *arXiv preprint arXiv:2310.19308*, 2023.
- Zhu, J., Wang, Y., Wu, L., Qin, T., Zhou, W., Liu, T.-Y., and Li, H. Making better decision by directly planning in continuous control. In *The Eleventh International Conference on Learning Representations*, 2023a. URL <https://openreview.net/forum?id=r8Mu7idxyF>.
- Zhu, Z., Zhao, H., He, H., Zhong, Y., Zhang, S., Yu, Y., and Zhang, W. Diffusion models for reinforcement learning: A survey. *arXiv preprint arXiv:2311.01223*, 2023b.

## A. Additional Related Works

**Hierarchical Planning.** Hierarchical frameworks are widely used in reinforcement learning (RL) to tackle long-horizon tasks with sparse rewards. Two main approaches exist: sequential and parallel planning. Sequential methods use temporal generative models, or world models (Ha & Schmidhuber, 2018; Hafner et al., 2019), to forecast future states based on past data (Li et al., 2022; Hafner et al., 2022; Hu et al., 2023; Zhu et al., 2023a). Parallel planning, driven by diffusion probabilistic models (Janner et al., 2022; Ajay et al., 2022), predicts all future states at once, reducing compounding errors. This has combined with hierarchical structures, creating efficient planners that train subgoal setters and achievers (Li et al., 2023; Kaiser et al., 2019; Dong et al., 2024; Chen et al., 2024a).

## B. Implementation Details

In this section, we describe the architecture and the hyperparameters used for our experiments.

- We build our code based on the official code release of Diffuser (Janner et al., 2022) obtained from <https://github.com/janner/diffuser> and official code release of HD (Chen et al., 2024b) obtained from <https://github.com/changchenc/Simple-Hierarchical-Planning-with-Diffusion>.
- We represent the level embeddings with a 2-layered MLP with a one-hot level encoding input. We condition the diffuser on the level embedding to generate multiscale trajectories. For training, we sample different levels and the level determines the resolution of the sampled trajectories.
- For the stitcher model, we train the diffuser with a short horizon  $H$  (Maze2D-Large: 80, Maze2D-Giant: 80, Maze2D-XXLarge: 80, Gym-MuJoCo: 10, Kitchen: 10)
- We represent the pondering depth predictor  $f_\phi^L(l|s_1, s_2)$  with a 3-layered MLP with 256 hidden units and ReLU activations. The classifier trained with samples from multiscale trajectories to predict the corresponding level.
- In practice, we define the maximum horizon that the model can plan as  $H_{\max} = H_L$ . Since the HMD model is shared across levels, the jump counts  $k_\ell$  remains fixed for all levels, that is  $k_\ell = k$  for all  $\ell$ . Consequently, the horizon of each level is given by:  $H_\ell = j_\ell \times k$ . As we predefine the jump lengths and as HMD at level  $\ell$  should plan with  $j_\ell$ , it is reasonable to establish a predefined order for the levels in the case of recursive calls. The Adaptive Plan Pondering (APP) mechanism is then used solely to determine the initial level at which to begin the planning process. Hence, it is not necessary to recursively call all levels to produce the dense plan.

## C. Details for long-horizon planning tasks

**Maze Layouts.** Our experiments are conducted on 3 maze-layouts varying in lengths, we used the Large Maze ( $9 \times 12$ ) from D4RL (Fu et al., 2020), the Giant Maze ( $12 \times 16$ ) from (Park et al., 2024), and designed a new XXLarge Maze ( $18 \times 24$ ) with a larger layout as shown in Figure C.5. The sizes are measured in maze block cells.

**Data Collection.** For data collection, we randomly sample start and goal locations within five maze cells to ensure short trajectories. Following D4RL, we collected one million transitions for each Maze setting and we call it the base dataset, as depicted in Figure C.5. Then, we run  $R$  rounds of PTE starting from the short base dataset.

**Training.** All models with -X suffix are trained with a fixed maximum planning horizon:  $H = 390$  for Large,  $H = 500$  for Giant, and  $H = 780$  for XXLarge. On the other hand, the Diffuser, trained only on the short base dataset, uses a planning horizon of  $H = 140$ , which corresponds to the mean trajectory length in the short dataset. For HMD, we use the hyperparameters as shown in Table C.4. For consistency, we set the maximum of the jump lengths for all environments to 15 to be equivalent to HD (Chen et al., 2024c). The jump count is determined by the highest jump length  $j_L$  and the planning horizon  $H$ .

**Evaluation.** We report the mean and standard error over  $N = 200$  seeds, the performance is measured by the normalized scores, scaled by a factor of 100 (Fu et al., 2020; Janner et al., 2022). Each maze has a maximum number of steps per episode,  $T = 800$  for Large,  $T = 1000$  for Giant, and  $T = 1300$  for XXLarge. As mentioned earlier in 5.2.1, we restrict the PD controller, Figure C.6 illustrates an example where the agent successfully reaches the goal even when the planning trajectory does not accurately lead to the goal.



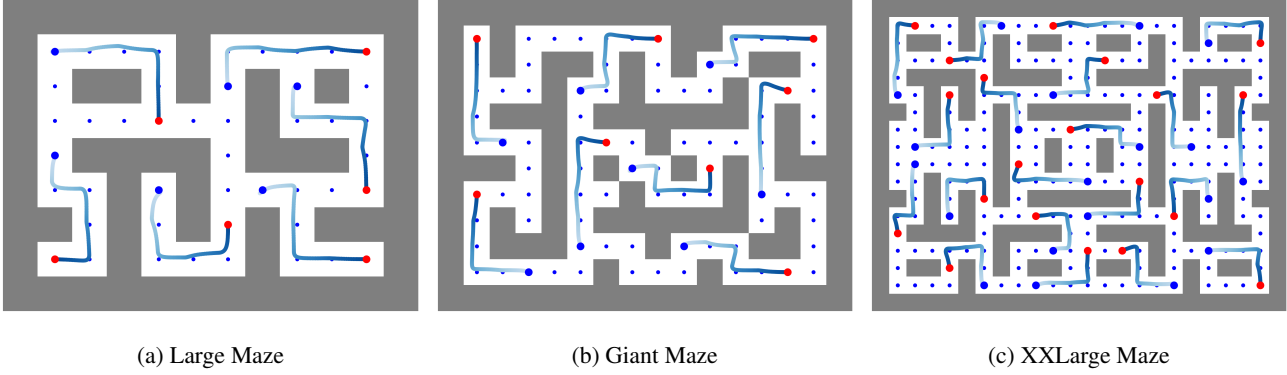


**Figure C.5:** A few examples of base trajectories for each maze configuration. Each small blue point represents the center of a corresponding maze cell. We randomly sampled start-goal pairs with a maximum distance of five maze cells and followed D4RL to collect base trajectories, resulting in a total of one million transitions in the Base dataset.

**Table C.4: Maze2D HMD Hyperparameters.**

Environment	Number of levels $L$	jump lengths $j_\ell$	jump count $k$
Large	4	(1, 8, 12, 15)	26
Giant	5	(1, 6, 9, 12, 15)	34
XXLarge	6	(1, 6, 8, 10, 12, 15)	52

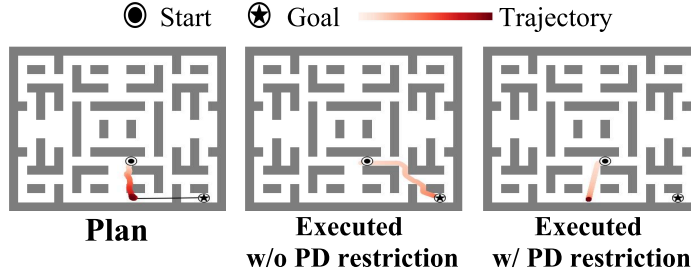


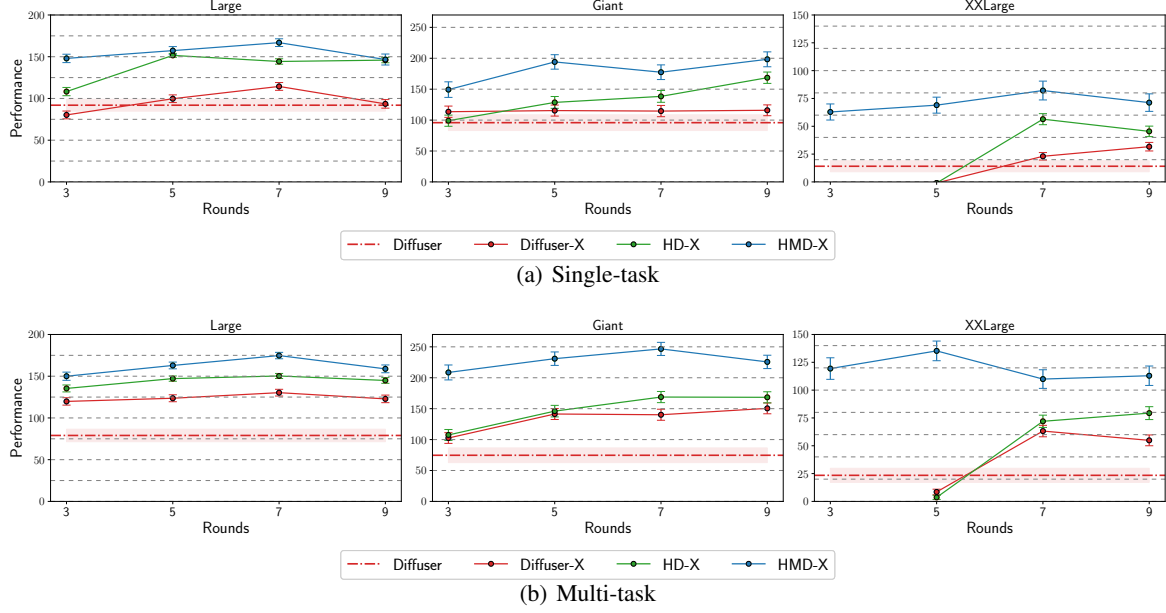
**Figure C.6:** An illustrative example for the PD controller restriction. This illustrates an example where the agent successfully reaches the goal even when the planning trajectory does not accurately lead to the goal.

### C.1. Additional results for Maze2D

We show in Figure C.7 the performance of the baselines with suffix -X that trained with various linear PTE rounds (3, 5, 7, 9). We use the union of rounds, for example, for round 3, we use the union of datasets collected of round 1, 2, and 3. The performance is generally increasing with more rounds. In XXL large, round 3 does not have the long trajectories enough to train Diffuser-X neither HD-X, but as HMD has multiscale planning horizons, it was able to train using the trajectories of round 3. The same reason applies of the bad results of round 5 for XXL large as the number of trajectories that Diffuser-X and HD-X with planning horizon  $H = 780$  are limited

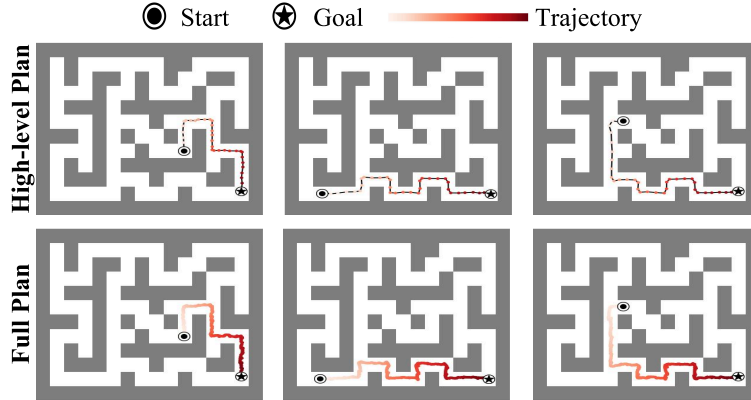
We present in Figure C.7 the performance of baselines with the -X suffix, trained using various rounds of linear PTE (3, 5, 7, 9). Training is conducted using the union of rounds; for example, performance shown in round 3, the models are trained with the dataset consists of trajectories collected from rounds 1, 2, and 3. Overall, performance improves with an increasing number of rounds. In the XXL large setting, round 3 does not contain sufficiently long trajectories to train Diffuser-X or HD-X. However, HMD-X, leveraging its multiscale planning horizons, is able to train using the available trajectories from round 3. A similar explanation applies to the poor performance of round 5 in XXL large. The number of available trajectories with a planning horizon of  $H = 780$  is limited, which affects the training of Diffuser-X and HD-X. Refer to Figure D.12 for the trajectories lengths across PTE rounds.

Figure C.8 illustrates the high-level plans generated by HMD when conditioned on the predicted level. Following this, HMD



**Figure C.7: Maze2D Performance.** We compare the performance of baselines in (a) single-task (Maze2D) and (b) multi-task (Multi2D) settings in various maze environments (Large, Giant, and XXLLarge). The -X baselines are trained with the extended dataset consists of the union of  $R$  rounds of Linear PTE, while Diffuser is only trained with the short base dataset. We report the mean and the standard error over 200 planning seeds. HMD-X consistently outperforms all baselines across all settings.

is recursively called at lower levels to generate the full plan (see Section 3.2.2).



**Figure C.8: Illustrative Examples of HMD's Hierarchical Planning and Full Generated Plans.** The high-level plan refers to the trajectory generated by HMD when conditioned on the predicted level. The full plan represents the final output of HMD after incorporating lower-level planning.

#### C.1.1. LONGER PLANNING HORIZONS.

In our previous experiments, the maximum planning horizon was 780 steps in the case of maze2d-xxlarge. To demonstrate the scalability of our approach for longer planning horizons, we conducted an experiment with a significantly extended planning horizon. Specifically, to address the constraints of limited maze layout sizes, we increased the planning horizon substantially by reducing the step size by a factor of five. This experiment was conducted in the Giant-Maze environment, where the planning horizon was extensively extended to 2400 steps. As the planning horizon increased, we also adjusted the maximum jump length for HMD-X to  $j_L = 120$ . Previously, we had set the maximum jump length to 15, as described in Table C.4

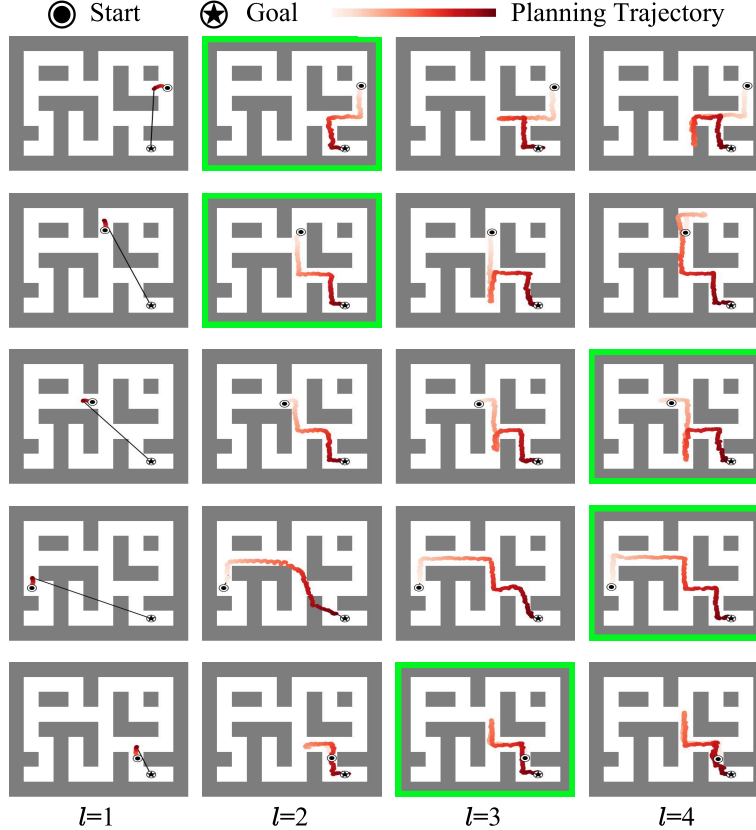


**Figure C.9: Multiscale trajectory planning using HMD with different levels ( $l$ ), where the figure highlighted with a green border indicates the level predicted by the pondering depth predictor.**

In Table C.5, we compare the performance of Diffuser-X, HD-X, and HMD-X trained with a planning horizon of 2400 steps. Our results show that HMD-X outperforms all baselines by a significant margin, whereas HD-X and Diffuser-X exhibit lower performance in comparison. Additionally, we trained a variant of HMD-X w/o multiscale planning. This baseline supports only three jump lengths (120, 12, 1) and during inference, the model iteratively conditions on these jumps to generate the final planned trajectory. This variant can be viewed as HD-X with a shared architecture or as HMD-X without multiscale planning. Our results indicate that HMD-X (No Multiscale) performs significantly worse than HMD-X, indicating the importance of multiscale planning.

**Table C.5: Longer Planning Horizons.** We compare the performance of baselines in single-task (Maze2D) and multi-task (Multi2D) settings in various maze environments (Giant-H2400) with a reduction in the step size by a factor of five. The baselines are trained with a planning horizon of 2400 steps. Additionally, we trained a variant of HMD-X w/o multiscale planning. This variant can be viewed as HD-X with a shared architecture or as HMD-X without multiscale levels.

Environment		Diffuser-X	HD-X	HMD-X	HMD-X (w/o multiscale)
Maze2D	Giant-H2400	98.8 $\pm$ 2.7	91.6 $\pm$ 4.6	<b>245.4 <math>\pm</math> 9.8</b>	94.0 $\pm$ 7.9
Multi2D	Giant-H2400	96.2 $\pm$ 2.8	88.1 $\pm$ 4.7	<b>225.5 <math>\pm</math> 10.0</b>	87.8 $\pm$ 8.3

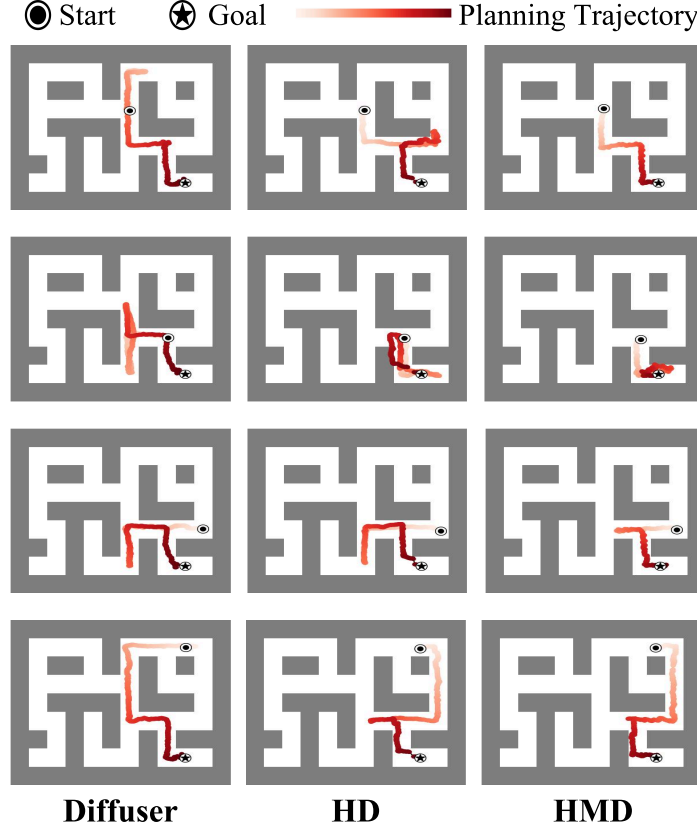


**Figure C.10: Comparison of planning trajectories using different models (Diffuser, HD, and HMD) illustrating variations in trajectory planning efficiency and goal-reaching performance.**

#### D. Progressive Trajectory Extension (PTE)

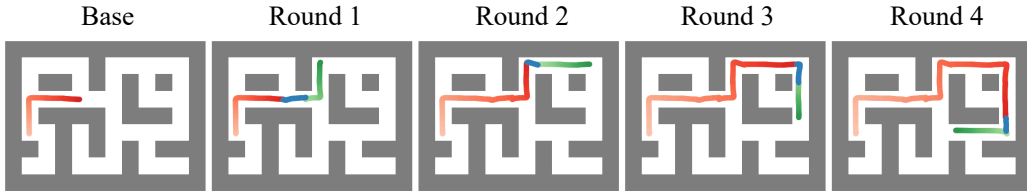


**Figure D.11: Linear PTE over multiple rounds, starting from a single base trajectory.** The current trajectory is shown in red, the bridge in blue, and the target trajectory in green. As rounds progress, the current trajectory is stitched to a new stitchable target trajectory sampled from the base dataset

In this section, we first provide the pseudocode of our Progressive Trajectory Extension (PTE) process in algorithm D.1. As discussed earlier, our PTE method allows flexible input datasets, thus enabling different stitching strategies. In algorithm D.2, we highlighted the process of linear PTE, and the exponential PTE is depicted in algorithm D.3. Additionally, Figure D.11 shows an illustration of the linear PTE over multiple rounds, starting from a single base trajectory. Furthermore, the trajectory length histograms for both Linear PTE and Exponential PTE are shown in Figure D.12.

##### D.1. Progressive Trajectory Extension (PTE) Pseudocode



**Algorithm D.1** Progressive Trajectory Extension

- 1: **Input:** Trained  $p_\theta^{\text{stitcher}}$ , Inverse Dynamic Model  $f_\theta^a$ , Reward Model  $f_\theta^r$ , Reachability Threshold  $\delta$ , Source Dataset  $\mathcal{S}^r$ , Target Dataset  $\mathcal{T}^r$ , Number of iterations  $N$
- 2: **Output:** Stitched Dataset  $D^r$
- 3: Initialize  $D^r := \emptyset$
- 4: **for**  $i = 1$  to  $N$  **do**
- 5:     Sample a source trajectory  $\tau^{\text{src}} \sim \mathcal{S}^r$  and a batch of target candidates  $\mathcal{T}_c \subset \mathcal{T}^r$
- 6:     Sample the last index  $t$  for the source trajectory  $\tau^{\text{src}}$  and a start index  $t'$  for each candidate  $\tau_i^{\text{cand}}$ .
- 7:     Obtain the source segment  $\tau_{0:t}^{\text{src}} := \tau_{0:t}^{\text{src}}$  and the target candidate segment  $\tau_i^{\text{cand}} := \tau_{i,t':\text{end}}^{\text{cand}}$  for each candidate.
- 8:     Sample a bridge trajectory  $\tau^{\text{brg}} \sim p_\theta^{\text{stitcher}}(\tau | s_0 = s_t^{\text{src}})$ , where  $s_t^{\text{src}}$  is the final state of the source trajectory  $\tau^{\text{src}}$ .
- 9:     Filter out candidate  $\tau_i^{\text{cand}}$  and get stitchable candidates  $\mathcal{T}_{\text{stitch}}$  based on:
 
$$\min_{t''} \text{dist}(s_{t''}^{\text{brg}}, s_{i,0}^{\text{cand}}) > \delta$$
- 10:     Randomly sample a target trajectory  $\tau^{\text{tgt}} \sim \mathcal{T}_{\text{stitch}}$
- 11:     Set  $k := \arg \min_{t''} \text{dist}(s_{t''}^{\text{brg}}, s_{i,0}^{\text{cand}})$
- 12:     Re-sample the bridge trajectory  $\tau^{\text{rebrg}} \sim p_\theta^{\text{stitcher}}(\tau | s_0^{\text{rebrg}} = s_t^{\text{src}}, s_{k:h}^{\text{rebrg}} = s_{0:h-k}^{\text{tgt}})$
- 13:     Initialize  $\tau_{\text{full}}^{\text{rebrg}} := \emptyset$
- 14:     **for**  $t = 0$  to  $k - 1$  **do**
- 15:         Predict action using the inverse dynamics model:  $a_t := f_\theta^a(s_t^{\text{rebrg}}, s_{t+1}^{\text{rebrg}})$
- 16:         Predict reward using the reward model:  $r_t := f_\theta^r(s_t^{\text{rebrg}}, a_t)$
- 17:         Append  $\{s_t^{\text{rebrg}}, a_t, r_t\}$  to  $\tau_{\text{full}}^{\text{rebrg}}$
- 18:     **end for**
- 19:     Get  $\tau^{\text{new}} := [\tau^{\text{src}}, \tau_{\text{full}}^{\text{rebrg}}, \tau^{\text{tgt}}]$
- 20:     Update  $D^r := D^r \cup \tau^{\text{new}}$
- 21: **end for**
- 22: **Return:** Extended Dataset  $D^r$

**Algorithm D.2** Linear PTE

- 1: **Input:** Trained  $p_\theta^{\text{stitcher}}$ , Inverse Dynamic Model  $f_\theta^a$ , Reward Model  $f_\theta^r$ , Reachability Threshold  $\delta$ , Previous Round Dataset  $\mathcal{D}_{\text{out}}^{r-1}$ , Base Dataset  $\mathcal{D}^0$ , Number of iterations  $N$
- 2: **Output:** Stitched Dataset  $D^r$   
     Use Algorithm D.1 with  $\mathcal{S}^r = \mathcal{D}_{\text{out}}^{r-1}$ ,  $\mathcal{T}^r = \mathcal{D}^0$
- 3: **Return:** Extended Dataset  $D^r$

**Algorithm D.3** Exponential PTE

- 1: **Input:** Trained  $p_\theta^{\text{stitcher}}$ , Inverse Dynamic Model  $f_\theta^a$ , Reward Model  $f_\theta^r$ , Reachability Threshold  $\delta$ , Previous Round Dataset  $\mathcal{D}_{\text{out}}^{r-1}$ , Number of iterations  $N$
- 2: **Output:** Stitched Dataset  $D^r$   
     Use Algorithm D.1 with  $\mathcal{S}^r = \mathcal{T}^r = \mathcal{D}_{\text{out}}^{r-1}$
- 3: **Return:** Extended Dataset  $D^r$

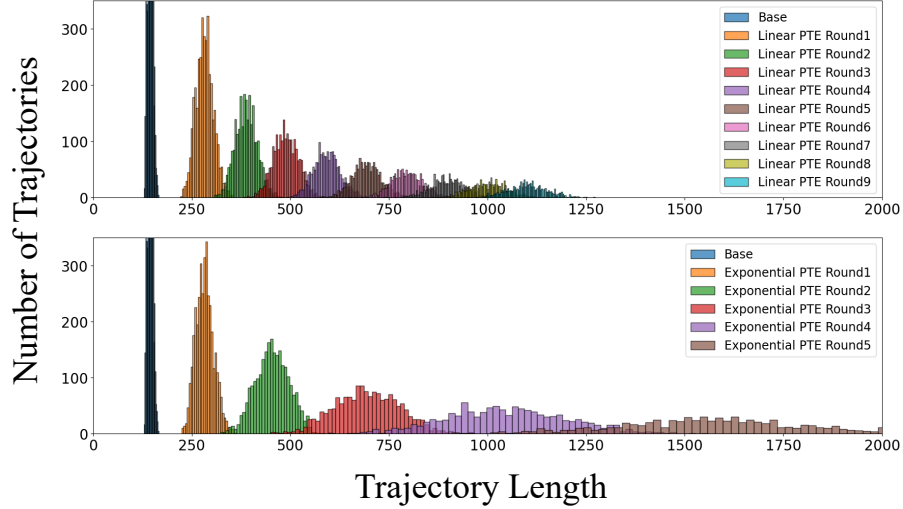


**Figure D.12: Comparison of Trajectory Length Histograms Across PTE Rounds in Maze2D-XXLarge.** Exponential PTE shows a more rapid increase in trajectory length, with earlier rounds producing longer maximum trajectories compared to Linear PTE. Linear PTE, on the other hand, demonstrates a steadier, more gradual extension across rounds.

## D.2. Planning with Recursive HM-Diffuser

We present the planning pseudocode with our proposed recursive HM-Diffuser in algorithm D.4 .

## D.3. Limits of PTE

It would be interesting to test the limits of our proposed PTE process. Intuitively, introducing a generative model during the extension introduces noise, making it straightforward to hypothesize that with successive rounds of extension, the planner might struggle to generate plausible plans due to the noisy dataset. We report our Kitchen results in Table D.6 and Gym-MuJoCo results in Table D.7. We report our results for the Kitchen in Table D.6 and for Gym-MuJoCo in Table D.7. To better understand the quality of our extended dataset, we include results from Diffuser trained on short segments of equivalent length from the original dataset (denoted as ‘No PTE’) for comparison. As shown in the tables, the performance of all models declines with more rounds of PTE, except for one exception in the Walker2d-MedExpert task, where HD-X and HMD-X achieved better performance after two rounds of PTE. Diffuser’s performance drops sharply as the planning horizon extends, whereas HD and HMD, benefiting from their hierarchical structure, remain more stable in comparison. We acknowledge this limitation and leave further investigation for future work.

**Table D.6:** Kitchen results from more rounds of PTE.

Task	length=10	length = 20				length = 40				length = 80			
	Base Trajectory	Round 1 PTE			No PTE	Round 2 PTE			No PTE	Round 3 PTE			No PTE
	Diffuser	Diffuser-X	HD-X	HMD-X	Diffuser	Diffuser-X	HD-X	HMD-X	Diffuser	Diffuser-X	HD-X	HMD-X	Diffuser
Kitchen-Partial	41.7 ± 3.2	43.3 ± 5.5	<b>56.7</b> ± 5.8	56.7 ± 5.3	35.8 ± 2.6	23.3 ± 6.3	<b>41.7</b> ± 2.9	<b>50.0</b> ± 3.9	26.7 ± 2.9	13.3 ± 3.1	40.0 ± 3.1	<b>45.0</b> ± 4.1	25.8 ± 2.8
Kitchen-Mixed	45.8 ± 3.1	48.3 ± 4.7	53.3 ± 3.1	<b>61.7</b> ± 3.1	40.8 ± 2.8	40.0 ± 5.4	<b>50.0</b> ± 3.9	50.0 ± 4.6	30.8 ± 4.2	18.3 ± 4.2	46.7 ± 4.5	<b>53.3</b> ± 5.0	32.5 ± 3.9
<b>Kitchen Average</b>	43.8	45.8	55.0	59.2	38.3	31.7	48.9	50.0	28.8	15.8	43.4	49.2	29.2

## E. Extended Kitchen and DMC Dataset and Training

**Extended Dataset.** To generate our extended dataset, we first construct the base dataset, which consists of short segments extracted from the standard D4RL dataset. Specifically, we partition the original D4RL offline dataset into non-overlapping segments of length 10. Next, we train a stitcher, implemented as a standard Diffuser, on this base dataset. To extend the trajectories, we uniformly sample a source trajectory and bridge it to a target trajectory, as described in Section 3.1. This process extends the trajectory lengths, which enables planning beyond the horizon of training dataset for diffusion-based

---

**Algorithm D.4** Planning with Recursive HM-Diffuser - Replanning
 

---

```

1: Input: HM-Diffuser  $p_\theta$ , Evaluation Environment  $env$ , Inverse Dynamic  $f_\theta^a$ , Number of Levels  $L$ , Jump Count
    $K = \{k_\ell\}^L$ 

2:  $s_0 = env.init()$ 
   ▷ Reset the environment.

3: done = False
4: while not done do
5:   for  $\ell$  in  $L, \dots, 1$  do
6:     if  $\ell == L$  then
7:        $\tau_g^\ell = \{g_0^\ell, \dots, g_{k_\ell}^\ell\} \leftarrow p_\theta(\tau | \ell, g_0^\ell = s_0)$ 
   ▷ Sample a subgoal plan given start.
8:     else
9:        $\tau_g^\ell = \{g_0^\ell, \dots, g_{k_\ell}^\ell\} \leftarrow p_\theta(\tau | \ell, g_0^\ell = s_0, g_{k_\ell}^\ell = g_1^{\ell+1})$ 
   ▷ Refine plans given subgoals from one layer above.
10:    end if
11:  end for
12:  Extract the first two states,  $s_0, s_1 = g_0^1$ , from the first layer plan  $\tau_g^1$ 
13:  Obtain action  $a = f_\theta^a(s_0, s_1)$ 
14:  Execute action in the environment  $s, done = env.step(a)$ 
15: end while
    
```

---



---

**Algorithm D.5** Recursive HM-Diffuser Training
 

---

```

1: Input: Recursive HM-Diffuser  $p_\theta$ , Inverse Dynamic  $f_\theta^a$ , number of levels  $L$ , Reward Model  $f_\theta^r$ , Jumpy Step Schedule
    $J = \{j^0, \dots, j^L\}$ , Training Dataset  $\mathcal{D}$ 
2: while not done do
3:   Sample a batch of trajectory from dataset  $\tau = \{s_t, a_t, r_t\}^{t+h} \sim \mathcal{D}$ 
4:   Sample a level  $\ell \sim \text{Unifrom}[0, \dots, L]$ 
5:   Obtain the sparse trajectory for level  $\ell$ :  $\tau^\ell = (g_0^\ell, \dots, g_{k_\ell}^\ell)$ 
6:   Train HM-Diffuser with Equation 4
7:   Train inverse dynamics  $f_\theta^a$ 
8:   Train reward model  $f_\theta^r$ 
9: end while
    
```

---

**Table D.7:** Gym-MuJoCo results from more rounds of PTE.

Task	length=10	length = 20				length = 40			
	Base Trajectory	Round 1 PTE			No PTE	Round 2 PTE			No PTE
	Diffuser	Diffuser-X	HD-X	HMD-X	Diffuser	Diffuser-X	HD-X	HMD-X	Diffuser
Walker2d-MedReplay	22.8 $\pm$ 2.7	20.1 $\pm$ 4.3	<b>30.2</b> $\pm$ 5.9	29.6 $\pm$ 4.8	24.9 $\pm$ 4.4	19.5 $\pm$ 2.6	<b>27.5</b> $\pm$ 2.6	22.7 $\pm$ 2.4	22.4 $\pm$ 4.2
Walker2d-Medium	58.1 $\pm$ 5.6	62.6 $\pm$ 6.4	66.5 $\pm$ 4.3	<b>72.7</b> $\pm$ 2.5	24.9 $\pm$ 6.8	41.0 $\pm$ 7.8	<b>55.3</b> $\pm$ 6.1	48.5 $\pm$ 5.4	23.7 $\pm$ 6.3
Walker2d-MedExpert	82.3 $\pm$ 4.6	80.3 $\pm$ 3.7	<b>80.8</b> $\pm$ 2.9	79.3 $\pm$ 2.3	77.7 $\pm$ 10.4	65.1 $\pm$ 8.3	<b>85.1</b> $\pm$ 3.9	84.7 $\pm$ 4.6	61.7 $\pm$ 6.8
<b>Walker2d Average</b>	54.4	54.3	59.2	<b>60.5</b>	42.5	41.9	56.0	52.0	35.9
Hopper-MedReplay	18.7 $\pm$ 3.0	34.5 $\pm$ 6.2	22.5 $\pm$ 3.1	<b>37.3</b> $\pm$ 4.2	29.1 $\pm$ 4.4	22.9 $\pm$ 4.1	<b>36.5</b> $\pm$ 4.9	31.6 $\pm$ 3.3	25.7 $\pm$ 3.8
Hopper-Medium	45.6 $\pm$ 1.9	44.3 $\pm$ 3.5	44.1 $\pm$ 2.8	<b>44.9</b> $\pm$ 3.5	50.5 $\pm$ 3.8	<b>44.5</b> $\pm$ 2.2	34.9 $\pm$ 2.8	42.1 $\pm$ 2.6	42.7 $\pm$ 2.1
Hopper-MedExpert	61.4 $\pm$ 8.4	<b>74.9</b> $\pm$ 8.0	67.9 $\pm$ 7.7	74.3 $\pm$ 9.0	61.3 $\pm$ 7.4	48.7 $\pm$ 4.8	<b>46.4</b> $\pm$ 5.3	<b>60.8</b> $\pm$ 8.5	52.2 $\pm$ 3.5
<b>Hopper Average</b>	41.9	51.2	44.8	<b>52.2</b>	46.6	38.7	39.3	<b>44.8</b>	40.2

planners. We generate a dataset of the same size as the standard offline dataset for Gym-MuJoCo and three times the size for Kitchen.

**Training.** We follow the training protocol as in Diffuser and HD. We deploy a two-layer HMD on Kitchen and Gym-MuJoCo, with  $j_2 = 4$  and  $j_1 = 1$ . The planning horizon the set to be the minimum length of the extended trajectory, i.e.  $H = 20$  for round 1 extension,  $H = 40$  for round 2 extension, and  $H = 80$  for round 3 extension.

## F. Additional Results

### F.1. Effects of Planning Horizon on Diffuser

We provide the results from Diffuser on dataset with varied segment length in Table F.8. The Infinite denotes the original setting, where the trajectory return is computed till the end of the episode.

**Table F.8:** Gym-MuJoCo performance with varied planning horizon.

Environment		H5	H10	Infinite
Walker2D	MedReplay	21.2 $\pm$ 8.1	22.8 $\pm$ 2.7	76.1 $\pm$ 5.0
Walker2D	Medium	60.2 $\pm$ 3.2	58.1 $\pm$ 5.6	81.8 $\pm$ 0.5
Walker2D	MedExpert	75.9 $\pm$ 4.3	82.3 $\pm$ 4.6	106.5 $\pm$ 0.2
<b>Walker2D Average</b>		52.4	54.4	88.1
Hopper	MedReplay	24.3 $\pm$ 5.0	18.7 $\pm$ 3.0	93.6 $\pm$ 0.4
Hopper	Medium	43.9 $\pm$ 1.8	45.6 $\pm$ 1.9	74.3 $\pm$ 1.4
Hopper	MedExpert	59.2 $\pm$ 6.6	61.4 $\pm$ 8.4	103.3 $\pm$ 1.3
<b>Halfcheetah Average</b>		42.4	41.9	90.4
Halfcheetah	MedReplay	35.3 $\pm$ 3.7	34.8 $\pm$ 4.8	37.7 $\pm$ 0.5
Halfcheetah	Medium	39.1 $\pm$ 3.2	45.2 $\pm$ 3.3	42.8 $\pm$ 0.3
Halfcheetah	MedExpert	72.4 $\pm$ 6.8	69.4 $\pm$ 7.5	42.8 $\pm$ 0.3
<b>Halfcheetah Average</b>		48.9	49.8	56.5

### F.2. Performance on Standard Benchmark

We provide the results on standard D4RL benchmark in Table F.9.



**Table F.9: HMD on Standard Benchmark.** HMD noticeably outperforms HD and Diffuser on the Maze2D tasks and performs comparably to HD on Kitchen and Gym-MuJoCo tasks.

Environment		Diffuser	HD	HMD
Maze2D	Large	128.6 $\pm$ 2.9	155.8 $\pm$ 2.5	<b>177.3</b> $\pm$ 3.89
Maze2D	Giant	86.9 $\pm$ 8.4	173.9 $\pm$ 8.7	<b>209.4</b> $\pm$ 11.9
Maze2D	XXLarge	61.9 $\pm$ 4.6	137.1 $\pm$ 4.4	<b>146.7</b> $\pm$ 9.1
Sing-task Average		92.5	155.6	<b>177.8</b>
Multi2D	Large	132.1 $\pm$ 5.8	165.5 $\pm$ 0.6	<b>181.3</b> $\pm$ 4.1
Multi2D	Giant	131.7 $\pm$ 8.9	181.3 $\pm$ 8.9	<b>258.9</b> $\pm$ 10.4
Multi2D	XXLarge	86.7 $\pm$ 5.6	150.3 $\pm$ 4.2	<b>209.5</b> $\pm$ 8.8
Multi-task Average		116.8	165.7	<b>216.6</b>
Walker2D	MedReplay	70.6 $\pm$ 1.6	<b>84.1</b> $\pm$ 2.2	80.7 $\pm$ 3.2
Walker2D	Medium	79.9 $\pm$ 1.8	<b>84.0</b> $\pm$ 0.6	82.2 $\pm$ 0.6
Walker2D	MedExpert	106.9 $\pm$ 0.2	107.1 $\pm$ 0.1	<b>107.6</b> $\pm$ 0.7
Walker2D Average		85.8	<b>91.7</b>	89.9
Halfcheetah	MedReplay	37.7 $\pm$ 0.5	38.1 $\pm$ 0.7	<b>41.1</b> $\pm$ 0.2
Halfcheetah	Medium	42.8 $\pm$ 0.3	<b>46.7</b> $\pm$ 0.2	44.9 $\pm$ 1.1
Halfcheetah	MedExpert	88.9 $\pm$ 0.3	92.5 $\pm$ 1.4	90.6 $\pm$ 1.3
Halfcheetah Average		56.5	<b>59.1</b>	58.9
Hopper	MedReplay	93.6 $\pm$ 0.4	94.7 $\pm$ 0.7	<b>95.5</b> $\pm$ 0.9
Hopper	Medium	74.3 $\pm$ 1.4	<b>99.3</b> $\pm$ 0.3	99.2 $\pm$ 0.1
Hopper	MedExpert	103.3 $\pm$ 1.3	115.3 $\pm$ 1.1	113.6 $\pm$ 2.7
Hopper Average		90.4	<b>103.1</b>	102.8
FrankaKitchen	Partial	55.0 $\pm$ 10.0	<b>73.3</b> $\pm$ 1.4	71.5 $\pm$ 2.0
FrankaKitchen	Mixed	58.3 $\pm$ 4.5	71.5 $\pm$ 2.3	<b>71.8</b> $\pm$ 3.3
FrankaKitchen Average		56.7	<b>72.4</b>	71.7